RESEARCH PAPER

# CNF-ADRC for MacPherson strut quarter-car suspension model

Muhammed F. Alhelou* and Khaldoun M. Salloum

Department of IU-1, Bauman Moscow Higher Technical School, Moscow, Russia

**ABSTRACT**

In this paper, a new simple mathematical model of MacPherson strut suspension system is proposed. The proposed model overcomes the complexities introduced in the nonlinear models found in literature. In addition, a new ADRC approach is proposed to achieve as fast as possible and without overshoot transient process. This ADRC approach depends on replacing the ADRC control part with a composite non-linear feedback (CNF) controller. Simulating the control of the proposed mathematical model of MacPherson suspension, a comparison is carried out between the new proposed ADRC, the conventional ADRC, Sky-hook and LQR controllers. Simulation results illustrate that CNF-ADRC has the best handling and comfort performance for active and semi-active MacPherson suspension system with a drawback of introducing new frequency components in the control signal of semi-active suspension.

**Key words:** MacPherson strut, Skyhook, CNF-ADRC, LQR, Comfort, Handling, Mathematical model.

## 1. INTRODUCTION

It has been stated by [1] that the functions of a suspension system are to carry the static weight of the vehicle, to maximize the friction between the tires and the road surface, to provide steering stability with good handling (minimize body roll) and to ensure the comfort of the passenger (ability to smooth out a bump road). However, car suspension systems can be organized as independents and non-independents. In non-independent configuration, both right and left wheels attached to the same solid axle. When one wheel hits a bump in the road, its upward movement causes a slight tilt of the other wheel. In independent configuration, each wheel on the same axle could move vertically independently of the other.

Popular suspension systems are leaf-spring suspension and coil-spring suspension. In leaf-spring configuration, the spring is connected directly to the real axle of the vehicle in order to damp vibrations. On the other hand, car coil springs, also called suspension springs, are made with wide gap coils that compress to absorb impact when tires roll over a rough terrain. In addition to improving ride quality by reducing bounce, coil springs and struts are also critical components that give the car its height and keep it off the ground. Coil spring is the

most common type of springs found in modern vehicles. It has the advantages of low cost and impact size over leaf-spring. Independent suspension used for front wheels is known as front-wheel independent suspension whereas the independent suspension used for rear wheels is known as rear-wheel independent suspension. Front-wheel independent suspension is mainly of five types: Double wishbone, MacPherson, Vertical guides, Training link and Swinging half axle and they are all coil-spring suspensions [2]. Typical MacPherson type suspension can be shown as in Fig.1 (a).

It consists of a single lower wishbone arm which is hinged to the chassis of the automobile. The other end of this wishbone arm is attached to the strut through a joint. The strut which contains the shock absorber and the spring is connected to the stub axle which carries the wheel. The upper end of this strut is fixed to the body structure through a flexible mounting (usually via a spherical link). Due to this a stronger body is required to absorb the full suspension load. Therefore frame-less chassis construction is preferred for this suspension (see Fig.2. The steering motion of the wheel is provided through the lower control arm. MacPherson strut suspension is very easy and cheap in construction and requires very less maintenance. It is lighter and simpler than double wishbone suspension thus keeping the unsprung weight lower. It requires very less space and so is very useful in front wheel driven automobiles where more room is required in the engine compartment [3].

However, different car alignment angles (mainly camber, caster and toe) are identified historically to describe their effect on the common steering problem. Camber is defined as inward or outward tilt of the wheel at the top when viewed from the front of the vehicle[4]. Camber is measured usually in degrees and a wheel with zero degrees camber is vertical. When a wheel tilts outward at the top it has positive camber and when a wheel is tilted inward at the top it has negative camber.

Suspension systems can be classified into three main categories: Passive, semi-active and active [5]. Passive suspensions include mainly the springs and shock absorbers. Semi-active depends on the changing of the shock absorber geometry so it could change its damping efficiency according to driving conditions. Semi-active damper could be seen as orifice-based damper or MR fluid-based damper. Active suspension includes additional damping parts

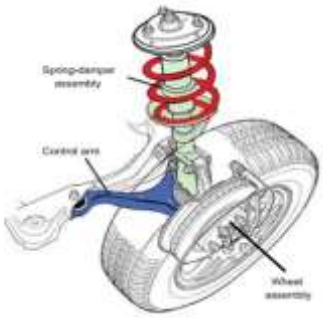


(a) MacPherson type suspension [11]

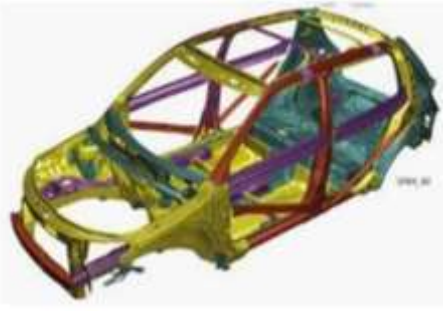

(b) Frame-less chassis [21]

**Fig 1. Front wheel independent MacPherson strut suspension**

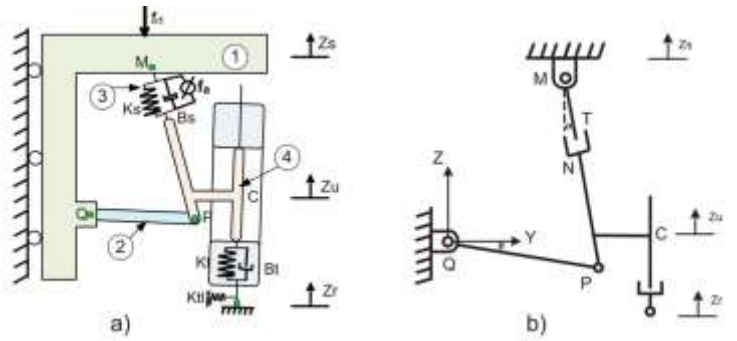


**Fig 2. MacPherson strut active suspension model [11]**

(new damping geometry). It could be seen as slow active, active or full active. Many works [6][7] focused on the mathematical modeling of MacPherson strut suspension system, while other works [8][9][10] were intended to study the effect of control action to active or semi-active MacPherson suspension system.

However, the contribution of this article summarizes three main points:

- Developing a new simple mathematical model describing the slow-active Macpherson suspension system to overcome the complexities of the nonlinear mathematical models found in literature.
- Introducing a new active disturbance rejection control (ADRC) approach that uses a composite non-linear feedback controller as its control part: (CNF-ADRC).
- Depending on the new mathematical model, a comparison is carried out between CNF-ADRC, Sky-hook, ADRC and a linear quadratic regulator (LQR) control system.

The effect of control signal saturation is analyzed by applying the two controllers in the case of semi-active suspension.

**Table 1. MacPherson strut suspension parameters values**

| Parameter | Meaning | Unit |
|---|---|---|
| $m\_s = 439.4$ | Sprung mass (chassis) | $Kg$ |
| $m\_t = 42.3$ | Unsprung mass (tyre) | $Kg$ |
| $K\_s = 38404.0$ | Suspension stiffness | $N/m$ |
| $B\_s = 3593.4$ | Suspension damping | $N.s/m$ |
| $K\_t = 310000.0$ | Tyre vertical stiffness | $N/m$ |
| $K\_tl = 190000.0$ | Tyre lateral stiffness | $N/m$ |
| $B\_t = 3100$ | Tyre damping | $N.s/m$ |
| $R = 0.3$ | Tyre effective radius | $m$ |
| $I\_C = 1.0$ | Wheel inertia moment on X-axis | $Kg.m\text{^}2$ |

RESEARCH PAPER

## 2. MACPHERSON STRUT ACTIVE SUSPENSION MODEL

We will depend on the model proposed in [11]. Fig.2 (a) shows a presentation of the proposed model. Typical MacPherson suspension system consists of the following parts: 1) Chassis, 2) Control arm, 3) Strut, 4) Wheel assembly.

$\theta$ is the control arm angle, $\alpha$ is the strut slope, $Z_s$ is the sprung mass displacement, $Z_u$ is the unsprung mass displacement, and $Z_r$ is the disturbance of the road. Table 1. shows the meaning and the values of the other parameters [11].

Fig 2. (b) presents the corresponding kinematic model as a four-bar mechanism, with suspension key points indicated by letters M, Q, P, C, T, and N. QYZ is the global reference frame in which QY is the horizontal axis and QZ is the vertical one. $Z_s, Z_u$ and $\theta$ are the states of this mechanism.

## 3. MODEL VALIDATION

The proposed model is valid in the following considerations [11]:

1. Chassis moves in vertical direction only.
2. All suspension system elements are rigid except the tyre.
3. Masses of the control arm and the suspension spring are negligible.
4. The wheel assembly is subjected to rotations and translations motions.
5. All joints are considered ideal.
6. Dampers and springs have linear behavior.
7. Strut slope does not change.

## 4. KINEMATIC MODEL

The suspension kinematics is analyzed using the displacement matrix method. The displacement matrix of the wheel can be formulated for a rotation about X-axis and translations on Y-axis and Z-axis. Suppose that the rotation is in order (Y-axis, Z-axis, X-axis), then we get:

$$R_x = \begin{bmatrix} cos(X) & sin(X) & 0 \\ -sin(X) & cos(X) & 0 \\ 0 & 0 & 1 \end{bmatrix} \quad (1)$$

And the displacement matrix will be:

$$[D]_{wheel}=\begin{bmatrix} cos(\phi) & sin(\phi) & Y_C-(cos(\phi)Y_{C0}+sin(\phi)Z_{C0}) \\ -sin(\phi) & cos(\phi) & Z_C-(-sin(\phi)Y_{C0}+cos(\phi)Z_{C0}) \\ 0 & 0 & 1 \end{bmatrix} \quad (2)$$

Where $\phi$ is the camber angle, $Y_C$ and $Z_C$ are instantaneous coordinates of the wheel center $C$, and $Y_{C0}$, $Z_{C0}$ correspond to their initial equilibrium values. The initial equilibrium state corresponds to a zero-camber angle where the vehicle model is defined by a set of constant positions of $M,Q,P,C,T,N.$ Points $N,T,P$ are supposed to be fixed to the wheel assembly, and the coordinates of them are $(Y_N,Z_N),(Y_T,Z_T),(Y_P,Z_P)$ respectively. Their initial coordinates are $(Y_{N0},Z_{N0})$ .,$(Y_{T0},Z_{T0}),(Y_{P0},Z_{P0})$. To express the movement of the point $N,T,P$ with respect to the origin $Q$, the wheel matrix displacement could be used as follows:

$$\begin{bmatrix} Y_N & Y_T & Y_P \\ Z_N & Z_T & Z_P \\ 1 & 1 & 1 \end{bmatrix}=[D]_{wheel}\begin{bmatrix} Y_{N0} & Y_{T0} & Y_{P0} \\ Z_{N0} & Z_{T0} & Z_{P0} \\ 1 & 1 & 1 \end{bmatrix} \quad (3)$$

By solving Eq.3, we get the following equations:

$$\begin{aligned} &Y_N-Y_C=a\cos(\phi)+b\sin(\phi),a=Y_{N0}-Y_{C0},b=Z_{N0}-Z_{C0} \\ &Y_T-Y_C=cc\cos(\phi)+d\sin(\phi),c=Y_{T0}-Y_{C0},d=Z_{T0}-Z_{C0} \\ &Y_P-Y_C=e\cos(\phi)+f\sin(\phi),e=Y_{P0}\quad Y_{C0},f=Z_{P0}-Z_{C0} \\ &Z_N=-a\sin(\phi)+Z_{N0}\cos(\phi)+Z_u,Z_u=Z_C-Z_{C0}\cos(\phi) \\ &Z_T=-c\sin(\phi)+Z_{T0}\cos(\phi)+Z_u \\ &Z_P=-e\sin(\phi)+Z_{P0}\cos(\phi)+Z_u \end{aligned} \quad (4)$$

Camber angle should be small in order to keep good contact with the road, so we could consider the following approximation: ( $cos(\phi)\approx 1, sin(\phi)\approx\phi$ ), thus we get:

| | |
|---|---|
| $Y_N - Y_C - b\phi = a$ | 5a |
| $Y_{T'} - Y_C - d\phi = c$ | 5b |
| $Y_P - Y_C - f\phi = e$ | 5c |
| $Z_N + a\phi = Z_{N0} + Z_u$ | 5d |
| $Z_{T'} + c\phi = Z_{T0} + Z_u$ | 5e |
| $Z_P + e\phi = Z_{P0} + Z_u$ | 5f |

Eq.5 describes the kinematic behavior of the wheel assembly (points $N, T, P$), but they do not account for points $M, Q$. However, System motion is illustrated in Fig.3 for the case of negative $Z_r$. $L_1$ is the length of the control arm, $L_2$ is the distance between Q and M, which are constants, $L_3$ is the length of the spring-damper assembly with initial value $L_{03}$, $\theta_0$ is the initial control arm angle, $\gamma_0$ is the initial angle between control arm and MQ and $\theta$ is the variation of control arm angle. This motion corresponds to a tyre deflection with lateral $\delta Y_t$ and vertical $\delta Z_t$ components. Two more equations are obtained from the system geometry:

$$Y_P = L_1 \cos(\theta_0 + \theta)$$
$$Z_P = L_1 \sin(\theta_0 + \theta) + Z_s$$

These two equations can be linearized as θ can be considered small:

| | |
|---|---|
| $Y_P + L\theta = m, \quad m = L_1 \cos(\theta_0), L = L_1 \sin(\theta_0)$<br>$Z_P - m\theta = L + Z_s$ | 6 |

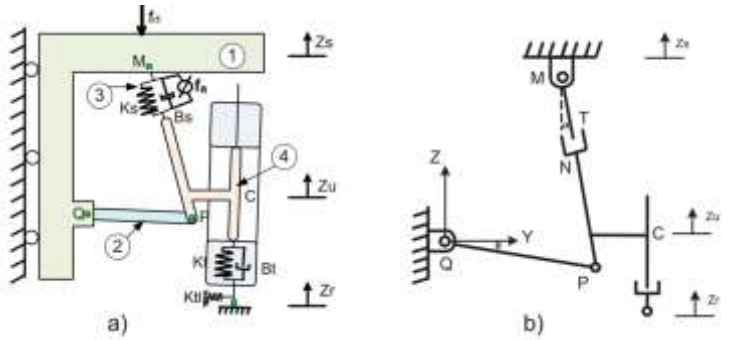


**Fig 3. MacPherson strut suspension motion state, ---initial configuration, __instantaneous**

And the last equation comes from the strict condition:

$$tan(\alpha) = \frac{Y_N - Y_T}{Z_N - Z_T} = \frac{Y_M - Y_P}{Z_M - Z_P}$$

Noting that the position of point $M$ is fixed relative to the point $Q$, and using Eq.5 and Eq.6 the last equation can be written in the form:

$$\frac{(b-d)\phi + (a-c)}{(b-d) - (a-c)\phi} = \frac{Y_{M0} + L\theta - m}{Z_{M0} - m\theta - L}$$

From this equation and by defining the following quantities:

$$X_1 = L(a-c) - m(b-d), \quad X_2 = (a-c)\left(Y_{M0} - m\right) - (b-d)\left(L - Z_{M0}\right)$$
$$X_3 = -L(b-d) - m(a-c), \quad X_4 = -(b-d)\left(Y_{M0} - m\right) - (a-c)\left(L - Z_{M0}\right)$$

We get:

$$X_1\theta\phi + X_2\phi + X_3\theta + X_4 = 0 \rightarrow \phi = -\frac{X_3\theta + X_4}{X_1\theta + X_2}$$

Using Taylor series and by neglecting the higher terms of θ (≥3) The resulted expression of the camber angle will be:

| | |
|---|---|
| $\phi = Y_3\theta^2 + Y_2\theta + Y_1$ | 7 |

where:

$$Y_1 = -\frac{X_4}{X_2}, \quad Y_2 = \frac{X_1X_4 - X_3X_2}{X_2^2}, Y_3 = \frac{X_1\left(X_2X_3 - X_1X_4\right)}{X_2^3}$$

Dynamical analysis requires three main solutions that are: $Y_C, \phi, \theta.$ To find these solutions, the following three equations are solved together:

| | |
|---|---|
| $Y_C + L\theta + f\phi + Z_1 = 0, \quad Z_1 = e - m$ | 8a |
| $m\theta + e\phi + Z_s - Z_u + Z_2 = 0, Z_2 = L - Z_{P0}$ | 8b |
| $\phi - Y_3\theta^2 - Y_2\theta - Y_1 = 0$ | 8c |

Eq.(8a) comes from Eq.(5c) and Eq.(8b) comes from Eq.(5f) while Eq.(8c) is Eq.7.However, by substituting Eq.(8c) in Eq.(8b) we get:

$$eY_3\theta^2 + (m + eY_2)\theta + eY_1 - Z_u + Z_s + Z_2 = 0 \quad (9)$$

Using Eq.9 the expressions of $Y_C$ and $\phi$ can be written in the form:

$$Y_C = \frac{f}{e}Z_s - \frac{f}{e}Z_u + N_1\theta + N_2,\ N_1 = \frac{fm}{e} - L,\ N_2 = \frac{fZ_2}{e} - Z1$$
$$\phi = -\frac{1}{e}Z_s + \frac{1}{e}Z_u - \frac{m}{e}\theta - \frac{Z_2}{e} \quad (10)$$

By differentiating Eq.9 with respect to time, the following equation could be achieved:

$$\dot{\theta}(m + eY_2 + 2eY_3\theta) = -\dot{Z}_s + \dot{Z}_u$$

It could be numerically (see Tab.1) easily verified that $m + eY_2 \gg 2eY_3\theta$ for small angles, so the last equation could be approximated by:

$$\dot{\theta} = -W_1\dot{Z}_s + W_1\dot{Z}_u,\ W_1 = \frac{1}{m + eY_2} \quad (11)$$

Eq.11 will be integrated later to get an approximation of θ. As a result, the velocities of the three main quantities can be expressed as:

$$\dot{\theta} = -W_1\dot{Z}_s + W_1\dot{Z}_u$$
$$\dot{Y}_C = W_2\dot{Z}_s - W_2\dot{Z}_u,\ W_2 = \frac{f}{e} - \frac{N_1}{m + eY_2}$$
$$\dot{\phi} = -W_3\dot{Z}_s + W_3\dot{Z}_u,\ W_3 = \frac{1}{eY_3} + \frac{N_3}{m + eY_2} \quad (12)$$

The tyre lateral deflection $\delta Y_{tl}$ is computed from $C$ position difference:

$$\delta Y_{tl} = (Y_C - \phi R) - Y_{C0} \quad (13)$$

The partially derivations of the last expression with respect to the generalized variables are:

$$\frac{\partial \delta Y_{tl}}{\partial Z_s} = \frac{\partial Y_C}{\partial Z_s} - R\frac{\partial \phi}{\partial Z_s} = S_1,\ S_1 = \frac{f+R}{e} - W_1(N_1 + \frac{Rm}{e})$$
$$\frac{\partial \delta Y_{tl}}{\partial Z_u} = \frac{\partial Y_C}{\partial Z_u} - R\frac{\partial \phi}{\partial Z_u} = -S_1 \qquad (14)$$

In the last equation the following approximations are used:

$$\frac{\partial \theta}{\partial Z_s} = -\frac{1}{m + eY_2 + 2eY_3\theta} \approx -W_1$$
$$\frac{\partial \theta}{\partial Z_u} \approx W_1$$

## 5. DYNAMIC MODEL

Non-formal education cannot able to fulfil the need of proper education and academic development of child but this education grip

$$T = \frac{1}{2}m_s\dot{Z}_s^2 + \frac{1}{2}m_u(\dot{Z}_u^2 + \dot{Y}_C^2) + \frac{1}{2}I_C\dot{\phi}^2$$
$$V = \frac{1}{2}K_s\delta\ell^2 + \frac{1}{2}K_tZ_t^2 + \frac{1}{2}K_{tl}\delta Y_{tl}^2 \qquad (15)$$
$$D = \frac{1}{2}B_s\delta\dot{\ell}^2 + \frac{1}{2}B_t\dot{Z}_t^2$$

Where $\delta\ell$ is the deflection of the spring-damper and $Z_t$ is the road disturbance error and they can be expressed as:

$$\delta\ell = L_3 - L_{03}$$
$$Z_t = Z_u - Z_r \qquad (16)$$

Using cosine law, expression of $\delta\ell$ could be written as:

$$L_3^2 = L_1^2 + L_2^2 - 2L_1L_2cos(\gamma_0 + \theta)$$
$$L_{03}^2 = L_1^2 + L_2^2 - 2L_1L_2cos(\gamma_0) \Rightarrow$$
$$L_3^2 = L_{03}^2 + k.\theta \Rightarrow \delta\ell = \sqrt{\Delta} - L_{03}$$
$$k = 2L_1L_2sin(\gamma_0), \Delta = L_{03}^2 + k.\theta$$

17

Using Taylor first order approximation, the expression of $\delta\ell$ can be simplified to:

$$\delta\ell = \frac{k}{2L_{03}}\theta$$

18

Now, using Lagrange method, the motion dynamic equations could be determined as follows:

Lagrange function: $\mathrm{L} = T - V$, Thus:

$$\mathrm{L} = \frac{1}{2}m_s\dot{Z}_s^2 + \frac{1}{2}m_u(\dot{Z}_u^2 + \dot{Y}_C^2) + \frac{1}{2}I_C\dot{\phi}^2 - \frac{1}{2}K_s\delta\ell^2 - \frac{1}{2}K_tZ_t^2 - \frac{1}{2}K_{tl}\delta Y_{tl}^2$$

19

Lagrange equation for the first coordinate:

$$\frac{d}{dt}\frac{\partial \mathrm{L}}{\partial \dot{Z}_s} - \frac{\partial \mathrm{L}}{\partial Z_s} + \frac{\partial D}{\partial \dot{Z}_s} = -f_d$$

20

Where $f_d$ is the external disturbance and:

$$\frac{\partial \mathrm{L}}{\partial \dot{Z}_s} = \zeta_1\dot{Z}_s - \zeta_2\dot{Z}_u$$

21

$$\frac{\partial \mathrm{L}}{\partial Z_s} = \zeta_3\theta - K_{tl}S_1Y_C + K_{tl}S_1R\phi + K_{tl}Y_{C0}S_1$$
$$\frac{\partial D}{\partial \dot{Z}_s} = \zeta_4\dot{Z}_s - \zeta_4\dot{Z}_u$$

22

Where:

$$\zeta_1 = m_s + m_u W_2^2 + I_C W_3^2,\ \ \zeta_2 = m_u W_2^2 + I_C W_3^2$$
$$\zeta_3 = \frac{K_s k^2 W_1}{4L_{03}^2},\ \ \zeta_4 = \frac{B_s k^2 W_1^2}{4L_{03}^2}$$

As a result, the first dynamic equation will be:

$$\zeta_1 \ddot{Z}_s - \zeta_2 \ddot{Z}_u - \zeta_3 \theta + K_{tl} S_1 Y_C - K_{tl} S_1 R\phi - K_{tl} Y_{C0} S_1 + \zeta_4 \dot{Z}_s - \zeta_4 \dot{Z}_u = -f_d \quad (23)$$

Applying Lagrange's equation with the second generalized coordinate $Z_u$:

$$\frac{d}{dt}\frac{\partial \mathrm{L}}{\partial \dot{Z}_u} - \frac{\partial \mathrm{L}}{\partial Z_u} + \frac{\partial D}{\partial \dot{Z}_u} = -f_a$$

Where $f_a$ is the control input and:

$$\frac{\partial \mathrm{L}}{\partial \dot{Z}_u} = -\zeta_2 \dot{Z}_s + \zeta_5 \dot{Z}_u$$
$$\frac{\partial \mathrm{L}}{\partial Z_u} = -\zeta_3 \theta + K_{tl} S_1 Y_C - K_{tl} S_1 R\phi - K_{tl} Y_{C0} S_1 - K_t Z_t$$
$$\frac{\partial D}{\partial \dot{Z}_u} = -\zeta_4 \dot{Z}_s + \zeta_4 \dot{Z}_u + B_t \dot{Z}_t \quad (24)$$

Where $\zeta_5 = m_u + m_u W_2^2 + I_C W_3^2$. As a result, the second dynamic equation will be:

$$-\zeta_2 \ddot{Z}_s + \zeta_5 \ddot{Z}_u + \zeta_3 \theta - K_{tl} S_1 Y_C + K_{tl} S_1 R\phi + K_{tl} Y_{C0} S_1 + K_t Z_t - \zeta_4 \dot{Z}_s + \zeta_4 \dot{Z}_u + B_t \dot{Z}_t = -f_a \quad (25)$$

Regarding Eq.23, Eq.25 and Eq.12, the full system dynamics can be rewritten in the form:

$$\zeta_1\ddot{Z}_s-\zeta_2\ddot{Z}_u+\zeta_4\dot{Z}_s-\zeta_4\dot{Z}_u+\zeta_6Z_s-\zeta_6Z_u+\zeta_7\theta+\zeta_8=-f_d \quad (26a)$$

$$-\zeta_2\ddot{Z}_s+\zeta_5\ddot{Z}_u-\zeta_4\dot{Z}_s+(\zeta_4+B_t)\dot{Z}_u-\zeta_6Z_s+(\zeta_6+K_t)Z_u-\zeta_7\theta-\zeta_8-B_t\dot{Z}_r-K_tZ_r=-f_a \quad (26b)$$

$$\dot{\theta}=-W_1\dot{Z}_s+W_1\dot{Z}_u \quad (26c)$$

Where:

$$\zeta_6=K_{tl}S_1\frac{R+f}{e},\ \zeta_7=K_{tl}S_1(N_1+\frac{Rm}{e}),\ \zeta_8=K_{tl}S_1(N_2+\frac{RZ_2}{e})$$

**Table 2. Suspension key points at initial state**

| | | |
|---|---|---|
| $Y_{C0}=0.4279$ | $Z_{C0}=0.0388$ | $Y_{Q0}=0.0$ |
| $Z_{Q0}=0.0$ | $Y_{N0}=0.2341$ | $Z_{N0}=0.1803$ |
| $Y_{P0}=0.2490$ | $Z_{P0}=-0.0608$ | $Y_{T0}=0.2179$ |
| $Z_{T0}=0.3782$ | $Y_{M0}=0.2049$ | $Z_{M0}=0.5249$ |

Thus, $L_1$, $L_2$, $L_{03}$ and initial angles can be calculated as follows:

$$L_1^2=Z_{P0}^2+Y_{P0}^2$$
$$L_2^2=Z_{M0}^2+Y_{M0}^2$$
$$L_{03}^2=(Z_{M0}-Z_{P0})^2+(Y_{P0}-Y_{M0})^2$$
$$\theta_0=\arctan(\frac{Z_{P0}}{Y_{P0}})$$
$$\gamma_0=\arccos(\frac{L_1^2+L_2^2-L_{03}^2}{2L_1L_2}) \quad (27)$$

However, the conventional model that depicts the vertical motions of the sprung and the unsprung masses could be expressed in the following dynamics [12]:

$$m_s\ddot{Z}_s=-K_s(Z_s-Z_u)-B_s(\dot{Z}_s-\dot{Z}_u)+f_a-f_d$$
$$m_u\ddot{Z}_u=K_s(Z_s-Z_u)+B_s(\dot{Z}_s-\dot{Z}_u)+K_t(Z_u-Z_r)+B_t(\dot{Z}_u-\dot{Z}_r)-f_a \quad (28)$$

Fig.4 shows the conventional model vs the proposed one responses when the road disturbance is a double bump and the car is supposed to move at velocity of $45K/h$. The double bump is described by Eq.29 where $w$ is the sudden bump, $h$ is the bump height, $t_0$ is the initial moment the bump begins, $x_t$ is a time delay, $V$ is the car speed, $\eta$ is an arbitrary constant and $\lambda$ is the disturbance wavelength. Fig.4(a) shows the bump signal that corresponds to $V = 45Km/h, h = 0.1m, t_0 = 4s, \lambda = 1m, x_t = 1s$.

$$w(t) = \begin{cases} 0.5h(1-cos(\frac{2\pi V(t-t_0)}{\lambda})), & t_0 \le t \le t_0 + \frac{\lambda}{V} \\ 0.5\eta h(1-cos(\frac{2\pi V(t-t_0-x_t)}{\lambda})), & t_0 + x_t \le t_f \le t_0 + x_t + \frac{\lambda}{V} \\ 0 \quad otherwise \end{cases} \qquad (29)$$

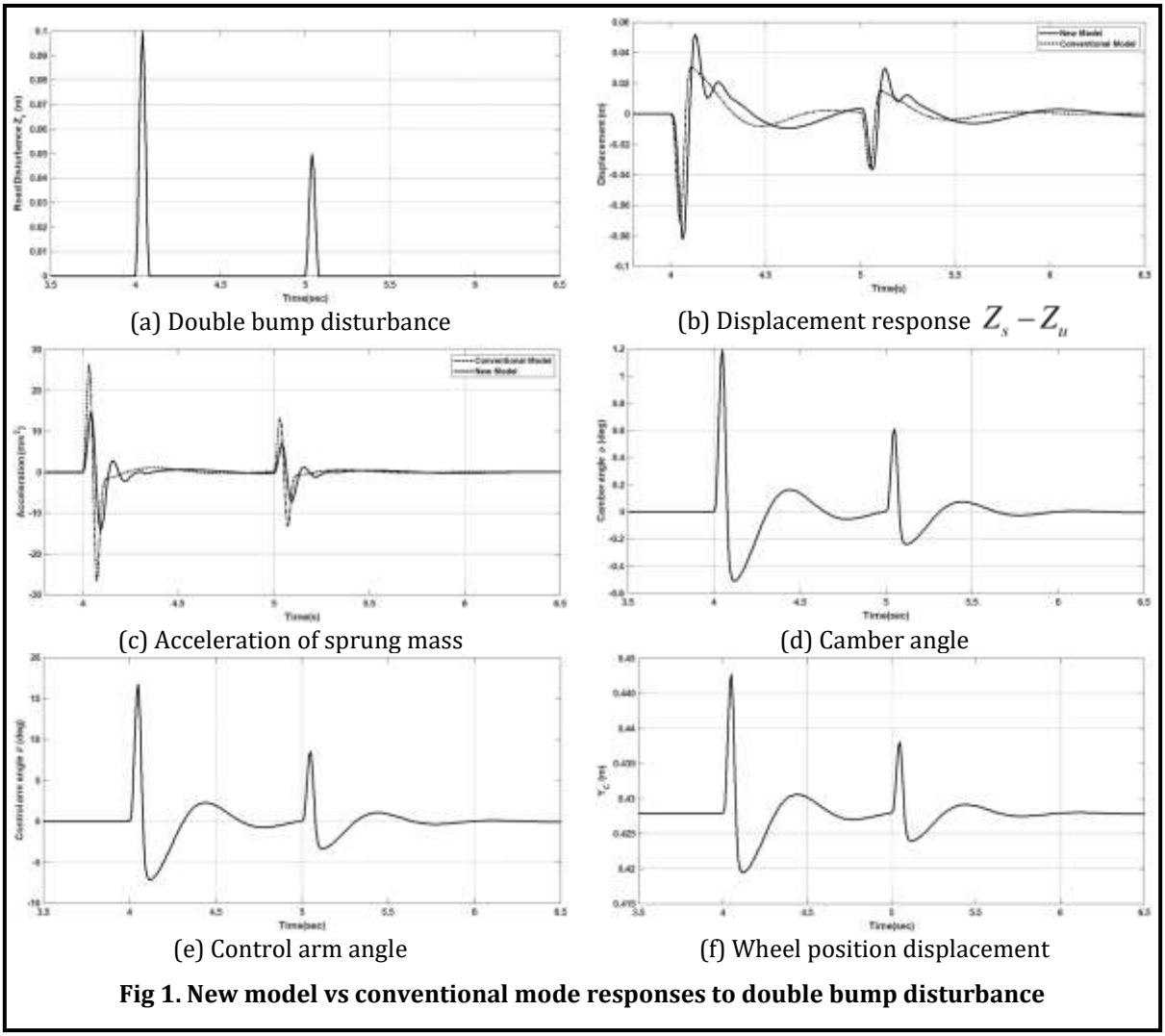


(a) Double bump disturbance

(b) Displacement response $Z_s - Z_u$

(c) Acceleration of sprung mass

(d) Camber angle

(e) Control arm angle

(f) Wheel position displacement

**Fig 1. New model vs conventional mode responses to double bump disturbance**

## 6. SECOND ORDER LINEAR ADRC (LADRC)

A lot of works [13][14][15][16] intended to study ADRC and show its possibilities and advantages over PID or LQR controllers. A linear ADRC consists of three main blocks: the controller, the linear estimator (Linear Extended State Observer (LESO)), the linear tracking differentiator (LTD) and a disturbance rejection scheme. Fig.5 shows a typical linear ADRC scheme. LTD is used to smooth out the reference signal using the signal velocity and a speed factor.

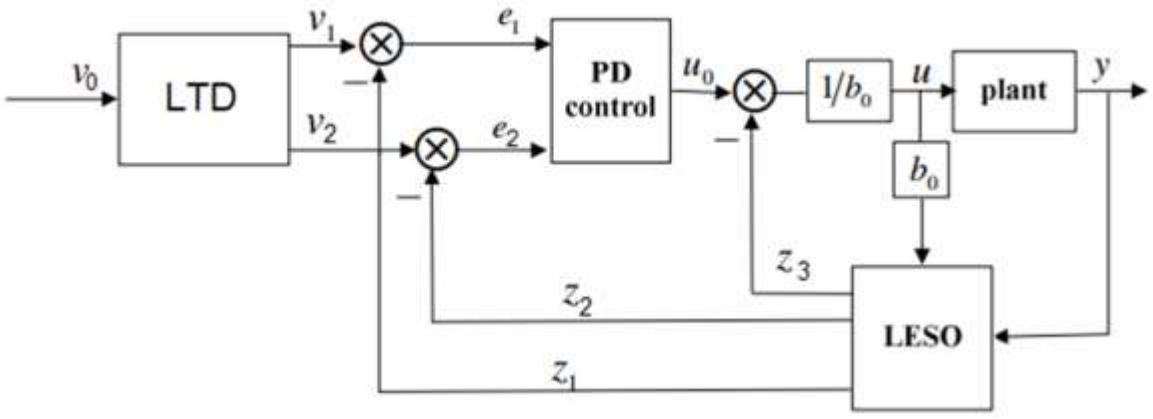


**Fig 5. Linear ADRC scheme**

LESO captures the information about the generalized disturbances and the internal dynamics of the system, while the control part is formulated depending on the observer outputs and the disturbance rejection scheme. In this paper, the reduced order LESO that proposed in [17] is used, while the controller will be a composite nonlinear feedback (CNF) one that is described in [18].

## 7. REDUCED ORDER LESO

For the reduced order LESO, the plant output is passed directly to the control scheme and the estimation is carried out for the output velocity and the external disturbances:

$$\begin{aligned} \dot{z}_2 &= z_3 + \hat{b}_0 u + \alpha_2(\dot{y} - z_2) \\ \dot{z}_3 &= \alpha_3(\dot{y} - z_2) \\ \dot{\hat{y}} &= z_2, \hat{f} = z_3 \end{aligned} \qquad (30)$$

Where $\alpha_1, \alpha_2, \alpha_3$ are the observer gains and $\hat{b}_0$ is an empirical constant.

## 8. CNF DESIGN FOR SECOND ORDER ADRC

We know that the ADRC method depends on estimating and isolating the nonlinear parts and external disturbances that are applied to the system under study and converting it into a system equivalent to a order integrator. That is, the new system can be viewed as a linear system without external disturbance.

This way, the control part in the ADRC can be replaced with a CNF one taking into consideration that the studied system is a second or higher order integrator and without disturbance; i.e, there no need for the auxiliary system.

However, in this section we will focus on the second order ADRC; i.e, designing a CNF controller for a second order integrator equivalent system with a set point target reference. Following the design steps in [18], we get:

Writing the linear system in vector-matrix form

$$A=\begin{bmatrix}0 & 1\\ 0 & 0\end{bmatrix},\ B=\begin{bmatrix}0\\ 1\end{bmatrix},\ C=\begin{bmatrix}1 & 0\end{bmatrix},\ D=0 \qquad (31)$$

**Step 2: Designing a state feedback gain matrix**

A state feedback gain matrix ( $K$ ) is designed to have as fast as possible transient process. If the system under study is a limited bandwidth (slow active) suspension system, hydraulic systems actively damp vertical chassis vibrations up to approx 5 Hz 19. However, $K$ is designed to have a transient process settle time of about $50\ ms$ . And the gain matrix $G$ can be calculated in the form:

$$G=\left[D-(C+DK)(A+BK)^{-1}B\right]^{-1} \qquad (32)$$

**Step 3: Lyaponov solution and scalar function**

A positive definite symmetric matrix $W$ can be chosen as: $W=\gamma\begin{bmatrix}1 & 0\\ 0 & 1\end{bmatrix}$ where $\gamma=const$ . This way, Lyaponov solution $P$ matrix can be calculated by solving the equation:

$$(A+BK)^{T}P+P(A+BK)=-W \qquad (33)$$

A scaled nonlinear function $\rho(e) = -\beta e^{-\alpha\alpha_0|e|}$ is used due its better performance robustness to variation of tracking targets. Here $e$ is the tracking error, $\alpha_0 = 1$ is chosen due to zero initial conditions in our case, $\alpha$ and $\beta$ can be chosen empirically to have the fastest and without overshoot transient response.

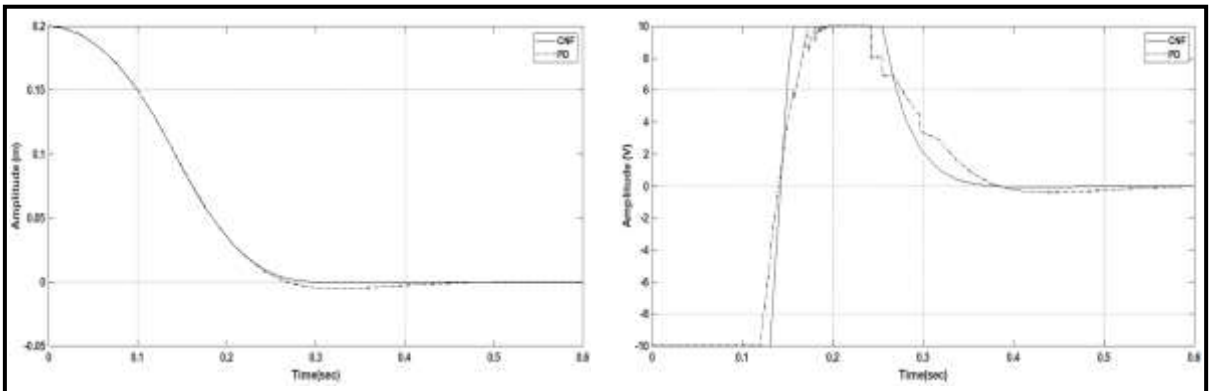


(a) Transient process of closed loop double integrator system

(b) Control signal of closed loop double integrator system

**Fig 6. CNF for double integrator system**

**Step 4: Gathering controller parts**

The whole controller parts are gathered together in the form:

$$u = K\begin{bmatrix} y & \dot{y} \end{bmatrix}^T + Gr + \rho(e)B^T P(y - r) \qquad (34)$$

Fig.6a shows the transient response for the double integrator system when is closed with a classical PD controller and a CNF controller to have similar performances in the presence of actuator saturation of $[-10,10]V$. Fig.6b shows the control signal in the two cases. It can be seen from the figure the smoothness of CNF control signal compared to the classical control one.

## 9. LQR DESIGN

From the dynamic's equations Eq.26, we get the following new expressions:

$$\begin{aligned}
\ddot{Z}_s &= \zeta\left\{\zeta_6(\zeta_2-\zeta_5)(Z_s-Z_u)-K_t\zeta_2(Z_u-Z_r)+\zeta_4(\zeta_2-\zeta_5)(\dot{Z}_s-\dot{Z}_u)\right.\\
&\left.-B_t\zeta_2(\dot{Z}_u-\dot{Z}_r)+\zeta_7(\zeta_2-\zeta_5)\theta-\zeta_2 f_a-\zeta_5 f_d+\zeta_8(\zeta_2-\zeta_5)\right\}\\
\ddot{Z}_u &= \zeta\left\{\zeta_6(\zeta_1-\zeta_2)(Z_s-Z_u)-K_t\zeta_1(Z_u-Z_r)+\zeta_4(\zeta_1-\zeta_2)(\dot{Z}_s-\dot{Z}_u)\right.\\
&\left.-B_t\zeta_1(\dot{Z}_u-\dot{Z}_r)+\zeta_7(\zeta_2-\zeta_5)\theta-\zeta_1 f_a-\zeta_2 f_d+\zeta_8(\zeta_1-\zeta_2)\right\}\\
\zeta &= \frac{1}{-\zeta_2^2+\zeta_1\zeta_5}
\end{aligned} \qquad (35)$$

As a result, if the following state variables are considered: $Z_s = x_1, \dot{Z}_s = x_2, Z_u = x_3, \dot{Z}_u = x_4$, the MacPherson strut dynamic equations can be expressed in state space as:

$$\begin{aligned}
\dot{x}_1 &= x_2\\
\dot{x}_2 &= f_1(x_1, x_2, x_3, x_4, f_a, Z_r)\\
\dot{x}_3 &= x_4\\
\dot{x}_4 &= f_2(x_1, x_2, x_3, x_4, f_a, Z_r)
\end{aligned} \qquad (36)$$

where $f_1 = \ddot{Z}_s$ and $f_2 = \ddot{Z}_u$.

These dynamic equations can be rewritten in the vector-matrix form:

$$\dot{x} = A_1 x + B_1 f_a + B_2 Z_r + B_3 \dot{Z}_r, \quad x = [x_1\ x_2\ x_3\ x_4]^T \qquad (37)$$

where the system matrix $A_1$, control input matrix $B_1$ and disturbance matrices $B_2, B_3$ are represented as:

$$A_1 = \begin{bmatrix} 0 & 1 & 0 & 0 \\ \frac{\partial f_1}{\partial x_1} & \frac{\partial f_1}{\partial x_2} & \frac{\partial f_1}{\partial x_3} & \frac{\partial f_1}{\partial x_4} \\ 0 & 0 & 0 & 1 \\ \frac{\partial f_2}{\partial x_1} & \frac{\partial f_2}{\partial x_2} & \frac{\partial f_2}{\partial x_3} & \frac{\partial f_2}{\partial x_4} \end{bmatrix},\ B_1 = \begin{bmatrix} 0 \\ \frac{\partial f_1}{\partial f_a} \\ 0 \\ \frac{\partial f_2}{\partial f_a} \end{bmatrix},\ B_2 = \begin{bmatrix} 0 \\ \frac{\partial f_1}{\partial Z_r} \\ 0 \\ \frac{\partial f_2}{\partial Z_r} \end{bmatrix},\ B_3 = \begin{bmatrix} 0 \\ \frac{\partial f_1}{\partial \dot{Z}_r} \\ 0 \\ \frac{\partial f_2}{\partial \dot{Z}_r} \end{bmatrix} \qquad (38)$$

Using Eq.35, we get:

$$\frac{\partial f_1}{\partial x_1} = \zeta\zeta_6(\zeta_2 - \zeta_5),\ \frac{\partial f_1}{\partial x_2} = \zeta\zeta_4(\zeta_2 - \zeta_5),\ \frac{\partial f_1}{\partial x_3} = -\zeta\zeta_6(\zeta_2 - \zeta_5) - K_t\zeta\zeta_2$$
$$\frac{\partial f_1}{\partial x_4} = -\zeta\zeta_4(\zeta_2 - \zeta_5) - B_t\zeta\zeta_2$$
$$\frac{\partial f_2}{\partial x_1} = \zeta\zeta_6(\zeta_1 - \zeta_2),\ \frac{\partial f_2}{\partial x_2} = \zeta\zeta_4(\zeta_1 - \zeta_2),\ \frac{\partial f_2}{\partial x_3} = -\zeta\zeta_6(\zeta_1 - \zeta_2) - K_t\zeta\zeta_1$$
$$\frac{\partial f_2}{\partial x_4} = -\zeta\zeta_4(\zeta_1 - \zeta_2) - B_t\zeta\zeta_1 \qquad (39)$$

With respect to the control signal we have:

$$\frac{\partial f_1}{\partial f_a} = -\zeta\zeta_2,\ \frac{\partial f_2}{\partial f_a} = -\zeta\zeta_1 \qquad (40)$$

With respect to the road disturbance:

$$\frac{\partial f_1}{\partial Z_r} = K_t\zeta\zeta_2,\ \frac{\partial f_2}{\partial Z_r} = K_t\zeta\zeta_1$$
$$\frac{\partial f_1}{\partial \dot{Z}_r} = B_t\zeta\zeta_2,\ \frac{\partial f_2}{\partial \dot{Z}_r} = B_t\zeta\zeta_1 \qquad (41)$$

The linear control law designed with LQR is given by:

$$f_a = -K_{LQR}x \qquad (42)$$

where $K_{LQR}$ is designed so that the damping-ratio of the resulting closed-loop system is more than 0.7 slightly.

## 10. SKY-HOOK DESIGN

In this control approach, the desired damping force is calculated to separate the function of sprung mass motion and the relative motion between sprung and unsprung masses, i.e:

$$f_a = \begin{cases} -D_{Sky}\dot{Z}_s & if\ \dot{Z}_s(\dot{Z}_s - \dot{Z}_u) > 0 \\ 0 & otherwise \end{cases} \quad (43)$$

It is important to note that a high pass filter is usually coupled with Sky-hook damper so the Sky-hook damper will not respond to constant velocities. In this work we considered a simple high pass filter with a cutoff frequency of about $0.5Hz$ thus it has the form:

$$Sky - Fil = \frac{s}{s + 3.14} \quad (44)$$

$D_{Sky} = 3000Ns/m$ is the Sky-hook gain. The Sky-hook control gain selection is made to have the best performance when the active actuator is limited to $[-4000, 4000]N$ for all control strategies.

## 11. SIMULATION RESULTS

Fig.7 shows different displacement outputs of MacPherson strut active suspension system when applying different control strategies and Fig.8 shows the sprung mass acceleration corresponding to these controllers.

It can be seen from the Fig (7,8) that the CNF-ADRC controller has the best performance.

However, to obtain a clearer comparison, we calculated the root mean square (RMS) of the deflection and the acceleration for each controller separately. These calculations correspond to different values of the double bump amplitude and vehicle speed. Tab.3 shows these calculations when the vehicle speed is and the disturbance length and Tab.4 shows these calculations when the vehicle speed is and the disturbance length.

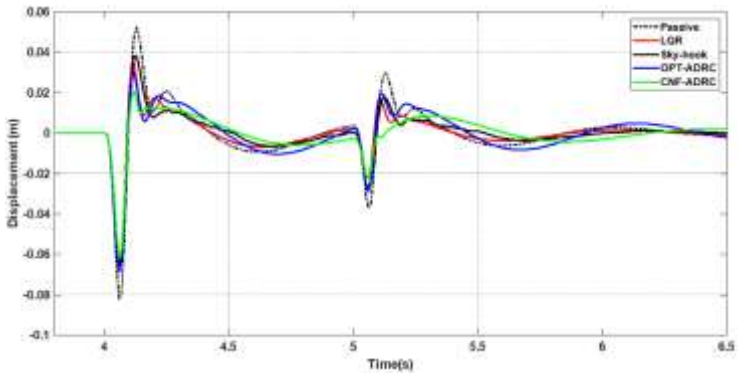


**Fig 7. Displacement response $Z_s - Z_u$ to double bump disturbance, V = 45Km/h**

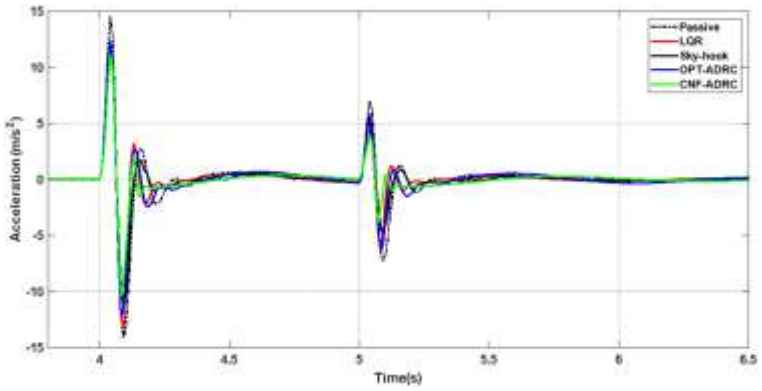


**Fig 8. Sprung mass acceleration response $\ddot{Z}_s$ to double bump disturbance, V = 45Km/h**

**Table 3. Displacement and Acceleration when $V = 25Km/h$**

$V = 25Km/h, \lambda = 1m, h[m], Dis[m], Acc[m/s^2]$

| | *LQR* | | *Sky - hook* | | *ADRC* | | *CNF - ADRC* | |
|---|---|---|---|---|---|---|---|---|
| | *Dis* | *Acc* | *Dis* | *Acc* | *Dis* | *Acc* | *Dis* | *Acc* |
| *h* = 0.1 | 0.0118 | 1.6547 | 0.0125 | 1.6411 | 0.0144 | 1.6277 | 0.0119 | 1.4068 |
| *h* = 0.07 | 0.0072 | 1.0066 | 0.0083 | 1.0812 | 0.0098 | 1.0987 | 0.0074 | 0.8054 |
| *h* = 0.05 | 0.0044 | 0.6053 | 0.0057 | 0.7194 | 0.0070 | 0.7848 | 0.0045 | 0.4436 |
| *h* = 0.02 | 0.0015 | 0.2043 | 0.0022 | 0.2786 | 0.0028 | 0.3139 | 0.0013 | 0.1088 |

**Table 4. Displacement and Acceleration when $V = 45Km/h$**

$V = 45Km/h, \lambda = 1m, h[m], Dis[m], Acc[m/s^2]$

| | *LQR* | | *Sky - hook* | | *ADRC* | | *CNF - ADRC* | |
|---|---|---|---|---|---|---|---|---|
| | *Dis* | *Acc* | *Dis* | *Acc* | *Dis* | *Acc* | *Dis* | *Acc* |
| h = *0:1* | 0.0084 | 1.6533 | 0.0090 | 1.6201 | 0.0100 | 1.7292 | 0.0079 | 1.3841 |
| h = *0:07* | 0.0052 | 1.0666 | 0.0060 | 1.0661 | 0.0068 | 1.1821 | 0.0049 | 0.7958 |
| h = *0:05* | 0.0033 | 0.6979 | 0.0041 | 0.7330 | 0.0048 | 0.8440 | 0.0030 | 0.4558 |
| h = *0:02* | 0.0012 | 0.2579 | 0.0016 | 0.2896 | 0.0019 | 0.3376 | 0.0007 | 0.0994 |

From these tables, the controllers can be arranged from best to worst for performance as follows: 1) CNF-ADRC, 2) LQR, 3) Sky-hock, 4) ADRC

## 12. EFFECT OF SATURATION (SEMI-ACTIVE SUSPENSION)

As we mentioned in the introduction, semi-active damper could be orifice based or magnetorheological fluid based. In orifice-based approach, suspension system makes use of an electrically controlled damping disc inside the shock absorber along with the springs to adjust the damping efficiency. When the motor shaft rotates, the number of opened orifice changes and the damping efficiency goes up or down. In general, the damping force of a semi-active damper is adjusted by changing the size of an orifice. The control input (damping force) is a function of the relative velocity and current input. Following [20], damping force characteristics of a typical continuously variable damper (CVD) could be drawn as in Fig.9(a).

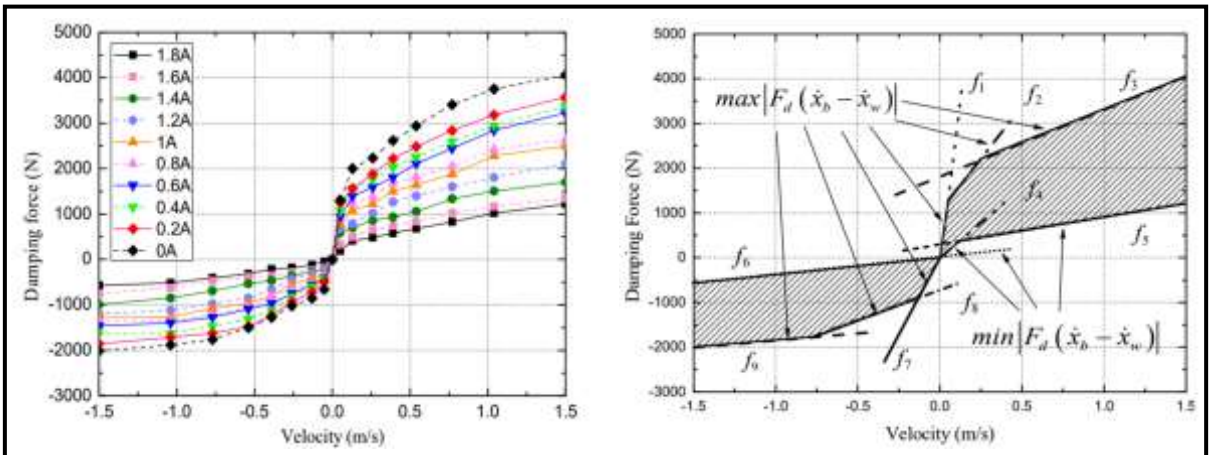


(a) Velocity-force map of semi-active CVD (b) Boundary model of semi-active CVD

**Fig 9. Typical semi-active damper characteristics**

Damping force is determined by the input current and the input velocity to the CVD. Boundary force corresponding to the control currents of $0A$ and $1.8A$ can be fitted piece-wise into nine straight lines, such as:

$$f_i = \alpha_i(\dot{x}_s - \dot{x}_u) + \beta_i, \quad i = 1,2,...,9 \qquad (45)$$

The boundary area and the nine lines of the adopted CVD are shown in Fig.9b. Parameters for each of these nine lines are listed in Tab.5. These boundaries were programmed in MATLAB and used to build a separate block which is then added to the front line of the control signal to express the limits imposed by the semi-active.

**Table 5. Parameters of boundary damper model of CVD**

| | $f_1$ | | $f_2$ | | $f_3$ | | $f_4$ | | $f_5$ | |
|---|---|---|---|---|---|---|---|---|---|---|
| $\dot{x}_s - \dot{x}_u > 0$ | $\alpha_1$ | $\beta_1$ | $\alpha_2$ | $\beta_2$ | $\alpha_3$ | $\beta_3$ | $\alpha_4$ | $\beta_4$ | $\alpha_5$ | $\beta_5$ |
| | 25154 | 0 | 4447 | 1077 | 1473 | 1850 | 3181 | 0 | 587 | 337 |
| | $f_1$ | | $f_2$ | | $f_3$ | | $f_4$ | | | |
| $\dot{x}_s - \dot{x}_u \leq 0$ | $\alpha_6$ | $\beta_6$ | $\alpha_7$ | $\beta_7$ | $\alpha_8$ | $\beta_8$ | $\alpha_9$ | $\beta_9$ | | |
| | 381 | 0 | 6592 | 0 | 1409 | -674 | 351 | -1489 | | |

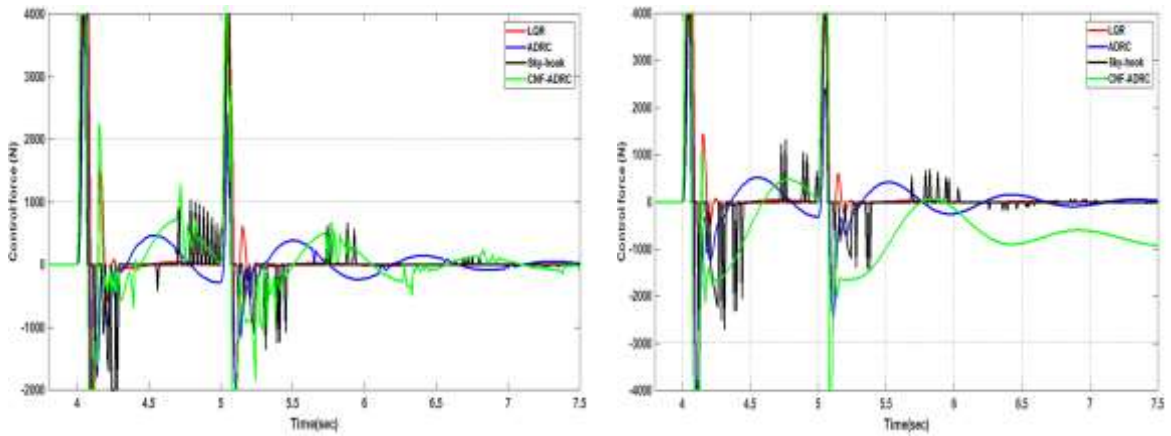


(a) Control-force of semi-active CVD (b) Control-force of active CVD

**Fig 10. Damping force of semi-active and active CVD response to double bump disturbance, V = 45Km/h**

Damper. Fig.10 shows the displacement output for vehicle speed of $45Km/h$ and bump height of $0.1m$. One can see that all controllers keep the same performance as for the active damper. However, Fig.11 shows the control force that needed to keep the same performance for every controller. It can be seen that new frequency components have been added to the control forces thus the controllers can be ranked from best to worst for smoothness as follows: 1) LQR, 2) ADRC, 3) CNF-ADRC, 4) Sky-hock.

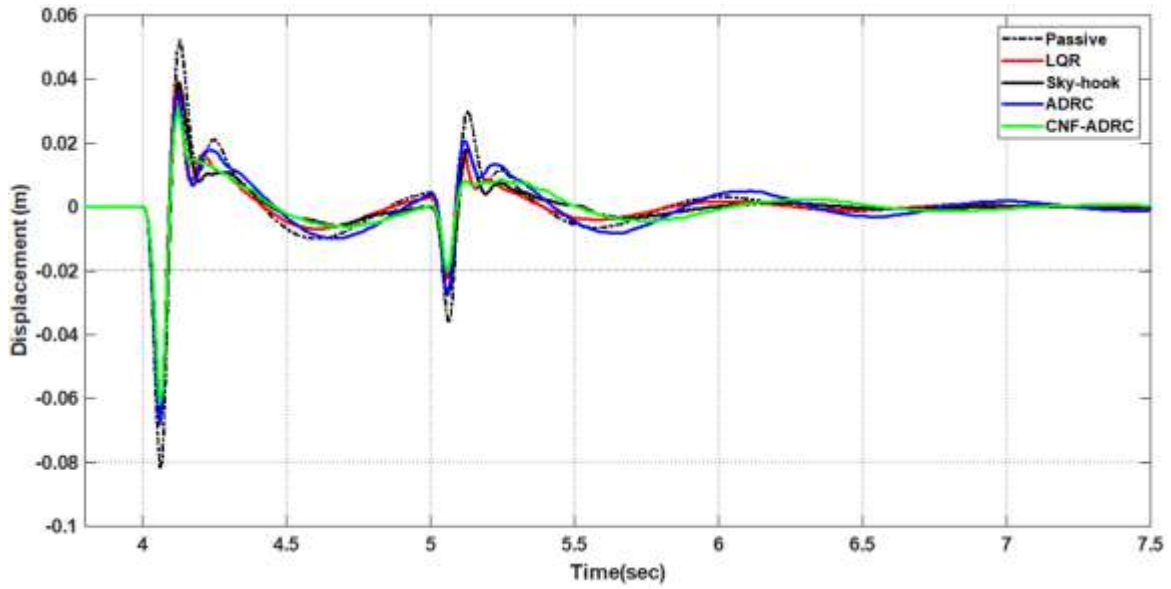


**Fig 11. Displacement of CVD response to double bump disturbance, V = 45Km/h**

## 13. CONCLUSION

Due to their favorable cost, simulation time, and low processing capacity requirements, mathematical models are widely used. This paper has presented a new and simple model of MacPherson suspension system that describes the vertical motion with the presence of camber and control arm angles. In addition, a new ADRC approach is proposed to enhance the transient process quality of the conventional ADRC. This method is based on replacing the control part of conventional ADRC with a composite nonlinear feedback one. To this end, a MATLAB simulation is performed to simulate the proposed mathematical model. The efficiency of four different control approaches to the mathematical model are tested: ADRC, CNF-ADRC, Sky-hook, and LQR. The simulation results demonstrated the following:

- CNF-ADRC has the best handling (displacement) and comfort (sprung mass acceleration) performances for active and semi-active suspensions.
- In the case of the semi-active system, new frequency components arose in the control signals where Skyhook was the worst and the LQR was the best in terms of the quality of the control signal.

It could be concluded that the control law of CNF-ADRC may be applicable to a semi-active suspension system without resulting in much degradation of control performance.

## 14. ACKNOWLEDGEMENT

NA

## 15. CONFLICT OF INTEREST

The authors have declared that there is no conflict of interest.

## 16. SOURCE/S OF FUNDING

No source of funding

## 17. REFERENCES


1. Donald Bastow, Geoffrey Howard, and John P Whitehead. Car suspension and handling. SAE international Warrendale, 2004.
2. P.E. Robert P. Tata. Automotive suspension systems. Continuing Education and Development, Inc, 2012.
3. SC Jain, Pushpendra kumar Sharma, and Dhara Vadodaria. Mcpherson suspension system-a review. International Journal For Technological Research In Engineering, *1***(12)**:29-35, 2014.
4. Stephen F Brauer and Nicholas J Colarelli III. Wheel alignment and diagnostic apparatus utilizing ride height, May 7 1996. US Patent *5*,513,439.
5. Mehrdad N Khajavi and Vahid Abdollahi (2007). Comparison between optimized passive vehicle suspension system and semi active fuzzy logic-controlled suspension system regarding ride and handling. In Proceedings of world academy of science, engineering and technology, *21*, pages 57-61.
6. MS Fallah, R Bhat, and Wen-Fang Xie (2008). New nonlinear model of macpherson suspension system for ride control applications. In 2008 American Control Conference, 3921-3926.
7. Jorge Hurel, Anthony Mandow, and Alfonso Garc´ıa-Cerezo (2012). Nonlinear two-dimensional modeling of a mcpherson suspension for kinematics and dynamics simulation. In 2012 12th IEEE International Workshop on Advanced Motion Control (AMC), 1-6.
8. Keum-Shik Hong, Dong-Seop Jeon, and Hyun-Chul Sohn (1999). A new modeling of the macpherson suspension system and its optimal pole-placement control. In Proceedings of the 7th Mediterranean Conference on Control and Automation (MED99), 559-579.
9. Saikat Dutta and Seung-Bok Choi. A nonlinear kinematic and dynamic modeling of macpherson suspension systems with a magneto-rheological damper. Smart Materials and Structures, *25***(3)**:035003, 2016.
10. S Sudin, YM Sam, K Peng, M Khairi Aripin, and M Fahezal Ismail (2014). Modeling and control of a nonlinear active suspension using multi-body dynamics system software.
11. Jorge Hurel, Anthony Mandow, and Alfonso Garc´ıa-Cerezo (2012). Nonlinear two-dimensional modeling of a mcpherson suspension for kinematics and dynamics simulation. In 2012 12th IEEE International Workshop on Advanced Motion Control (AMC), 1-6.
12. Faried Hasbullah, Waleed F Faris, Fadly Jashi Darsivan, and Mohammad Abdelrahman (2015). Ride comfort performance of a vehicle using active suspension system with active disturbance rejection control. International Journal of Vehicle Noise and Vibration, *11***(1)**:78-101
13. Jingqing Han. From pid to active disturbance rejection control. IEEE transactions on Industrial Electronics, 56(3):900-906, 2009.
14. Fengping Li, Zhengya Zhang, Antonios Armaou, Yao Xue, Sijia Zhou, and Yuqing Zhou (2018). Study on adrc parameter optimization using cpso for clamping force

control system. Mathematical Problems in Engineering

15. Wang Changshun, Zhang Huang, and You Yu (2017). Usv trajectory tracking control system based on adrc. In 2017 Chinese Automation Congress (CAC), 7534-7538.
16. Zhiqiang Gao and Gang Tian (2012). Extended active disturbance rejection controller, May 15. US Patent 8,180,464.
17. Jun Yang, Hongyu Cui, Shihua Li, and Argyrios Zolotas (2017). Optimized active disturbance rejection control for dc-dc buck converters with uncertainties using a reduced-order gpi observer. IEEE Transactions on Circuits and Systems I: Regular Papers, *65***(2)**:832-841.
18. Guoyang Cheng, Ben M Chen, Kemao Peng, and Tong H Lee (2010). A matlab toolkit for composite nonlinear feedback controlimproving transient response in tracking control. Journal of Control Theory and Applications, *8***(3)**:271-279.
19. Guido Koch, Oliver Fritsch, and Boris Lohmann (2010). Potential of low bandwidth active suspension control with continuously variable damper. Control Engineering Practice, *18***(11)**:1251-1262.
20. Zhushun Ding, Feng Zhao, Yechen Qin, and Cheng Tan (2017). Adaptive neural network control for semi-active vehicle suspensions. Journal of Vibroengineering, *19***(4)**:2654-2669.
21. Dixit, R., Kaushik, K., & Mittal, P. (2018). Modeling, analysis & optimization of parameters for great weld strength of the chassis for off-road vehicles. Int Res J Eng Technol, *5***(5)**, 1907-1915.